


Article

Modified Ferrocenes as Primary Driers for Formulations of Alkyd Paints

Jan Honzíček ^{1,*} , Tatiana Fedorova ¹, Jaromír Vinklárek ², Tomáš Mikysek ³ and Ivana Císařová ⁴

¹ Institute of Chemistry and Technology of Macromolecular Materials, Faculty of Chemical Technology, University of Pardubice, Studentská 573, 532 10 Pardubice, Czech Republic; st52637@student.upce.cz

² Department of General and Inorganic Chemistry, Faculty of Chemical Technology, University of Pardubice, Studentská 573, 532 10 Pardubice, Czech Republic; jaromir.vinklarek@upce.cz

³ Department of Analytical Chemistry, Faculty of Chemical Technology, University of Pardubice, Studentská 573, 532 10 Pardubice, Czech Republic; tomas.mikysek@upce.cz

⁴ Department of Inorganic Chemistry, Faculty of Science, Charles University in Prague, Hlavova 2030/8, 128 43 Prague 2, Czech Republic; cisarova@natur.cuni.cz

* Correspondence: jan.honzicek@upce.cz

Received: 6 August 2020; Accepted: 7 September 2020; Published: 9 September 2020



Abstract: The effect of modification of benzoylferrocene periphery on catalytic activity toward drying of alkyd resins has been investigated by the combination of experimental techniques. A series of substituted ferrocenes have been synthesized and characterized by analytical and spectroscopic tools including X-ray diffraction analysis on single crystals. The electrochemical behavior of the ferrocene derivatives has been elucidated by cyclic voltammetry and rotation disk voltammetry. The activity toward room temperature curing of alkyd resin has been evaluated by standard mechanical tests on coated plates, which enabled to establish a structure/catalytic activity relationship. Fast drying of test coatings has been observed for formulations of (3-methoxybenzoyl) ferrocene. Time-resolved infrared spectroscopy in combination with attenuated total reflectance sampling technique enabled to reveal the kinetic origin of the improved performance for this ferrocene derivative.

Keywords: ferrocene; air-drying paint; alkyd; drier; cobalt replacement; X-ray diffraction; autoxidation; electrochemistry

1. Introduction

Ferrocene, $[(\eta^5\text{-C}_5\text{H}_5)_2\text{Fe}]$, is under comprehensive scrutiny by many research groups due to its unique structural and electrochemical properties, easy derivatization and high thermal stability [1]. It has found many applications in various areas but the most prominent one is the use in catalysis. Chiral ferrocene-based ligands with tunable electronic properties are used for assembly of highly selective catalysts for asymmetric organic synthesis [2,3]. Ferrocene-containing polymers serve as burning rate catalysts for rocket propellants [4]. Ferrocene itself catalyzes benzene hydroxylation [5]. Mild and reversible redox process $\text{Fe}^{\text{II}}/\text{Fe}^{\text{III}}$ makes ferrocene a suitable catalyst of Fenton-like reactions, which are utilized for degradation of organic contaminants in wastewater e.g., dye pollutants or residual antibiotics [6–8]. Ferrocene and several acyl-substituted derivatives were used as photoinitiators for anionic polymerization of alkyl α -cyanoacrylate [9,10].

Our research group has been attended in application of ferrocene-based catalysts in the paint-producing industry. We focus mainly on curing of air-drying paints based on alkyd resins modified with vegetable oils. These binders fulfil current ecological requirements as the modifying component comes from renewable sources [11]. The main drawback of neat alkyd resins is a very slow

film-formation process. After fast evaporation of organic solvent, the chemical curing of solvent-borne alkyd paints proceeds very slowly as the process is based on autoxidation, modifying drying or semi-drying plant oil. In stoving enamels, such drawback is solved by curing at elevated temperature. Curing at room temperature is commonly accelerated by metal-based catalysts known as primary driers [12]. Cobalt-based driers are currently the most widespread paint-producing industry not only due to high catalytic power and low price but also due to well-tried combinations with solvents, pigments and additives such as secondary driers and anti-skinning agents [12]. Nevertheless, the quest for new powerful primary driers is still ongoing, owing to toxic effects of cobalt(II) compounds currently evaluated by European Chemical Agency [13,14]. Many alternatives for cobalt-based driers are reported in literature [12]. They involve various manganese [15,16], iron [17,18] and vanadium compounds [19–24]. Although some of them are commercially available, they often suffer from some drawbacks such as low activity, loss of activity during storage, dark coloration or poor reproducibility at non-standard conditions.

Ferrocene and several alkyl and ester-substituted derivatives show sufficient drying activity but only in conjunction with aforementioned cobalt-based driers [25]. Nevertheless, attachment of acyl function improves the performance of ferrocene considerably [26]. Recently, we have demonstrated promising activity of benzoylferrocene (**1**) in industrially used alkyd resin modified with semidrying soybean oil [27].

The aim of this study is to evaluate subtle structure/activity relationship on a series of modified benzoylferrocenes. The study includes synthesis, characterization and evaluation of drying activity using standard mechanical tests. Kinetic measurements by time-resolved infrared spectroscopy are also presented.

2. Experimental Section

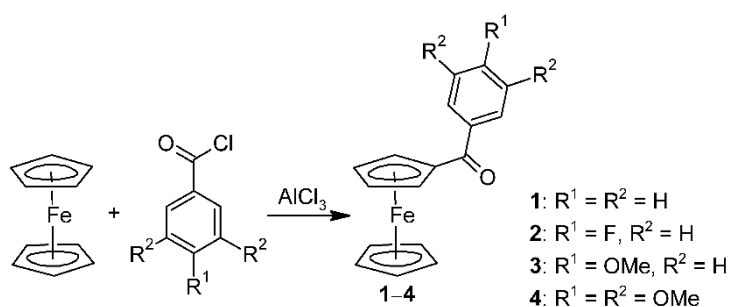
2.1. Materials and Methods

All synthetic operations were performed under protective atmosphere of nitrogen using standard vacuum/inert techniques. The solvents were purified and dried by standard methods [28]. $[(\eta^5\text{-C}_5\text{H}_4\text{COPh})(\eta^5\text{-C}_5\text{H}_5)\text{Fe}]$ (**1**) was prepared according to literature procedure [29]. Starting carboxylic acids were obtained from Acros Organics (Geel, Belgium). Alkyd resin CHS-ALKYD S471 X 60 (oil length 47%, acid value = 6 mg) was obtained from Spolchemie (Ústí nad Labem, Czech Republic).

The infrared spectra were recorded in mid region ($4000\text{--}400\text{ cm}^{-1}$) with resolution of 1 cm^{-1} on a Nicolet iS50 FTIR spectrometer (Thermo Scientific, Waltham, MA, USA) using a Diamond Smart Orbit ATR. ^1H and $^{13}\text{C}\{^1\text{H}\}$ NMR spectra were collected on a Avance 500 spectrometer (Bruker, Billerica, MA, USA) at room temperature. The chemical shifts are given in ppm relative to $(\text{CH}_3)_4\text{Si}$. Elemental composition (C, H, N) was analyzed on a Flash 2000 CHNS Elemental Analyzer (Thermo Scientific, Waltham, MA, USA).

2.2. Synthesis of Acyl Chlorides

For chemical structures, see Scheme 1 in the section “Results and Discussion”.



Scheme 1. Synthesis of acyl-substituted ferrocenes.

2.2.1. Synthesis of 4-Fluorobenzoyl Chloride

4-Fluorobenzoic acid (14.0 g, 100 mmol) was dissolved in CHCl_3 (25 mL), treated with SOCl_2 (25 mL) and heated for reflux for 2 h. After cooling to room temperature, all volatiles were vacuum evaporated on rotavapor. The reaction product was purified by vacuum distillation. Bp = 60 °C (3 Torr). Yield: 12.4 g (0.78 mmol, 78%). Analytical and spectroscopic data are in line with those reported elsewhere [30].

2.2.2. Synthesis of 4-Methoxybenzoyl Chloride

The steps of synthesis followed the aforementioned protocol for 4-fluorobenzoyl chloride, but starting from 4-methoxybenzoic acid (15.2 g, 100 mmol). Bp = 103 °C (3 Torr). Yield: 14.6 g (86 mmol, 86%). Analytical and spectroscopic data are in line with those reported elsewhere [31].

2.2.3. Synthesis of 3,4,5-Trimethoxybenzoyl Chloride

The steps of synthesis followed the aforementioned protocol for 4-fluorobenzoyl chloride but starting from 3,4,5-trimethoxybenzoic acid (21.2 g, 100 mmol). Yield: 17.5 g (76 mmol, 76%). Analytical and spectroscopic data are in line with those reported elsewhere [32].

2.3. Synthesis of Modified Ferrocenes

For chemical structures, see Scheme 1 in the section “Results and Discussion”.

2.3.1. Synthesis of (4-Fluorobenzoyl)ferrocene (2)

Ferrocene (2.0 g, 10.75 mmol) was dissolved in CH_2Cl_2 (25 mL), treated with AlCl_3 (1.8 g, 13.5 mmol) and cooled to 0 °C. The suspension was vigorously stirred and treated dropwise with 4-fluorobenzoyl chloride (1.8 g, 11.4 mmol), freshly prepared from 4-fluorobenzoic acid and thionyl chloride. The reaction mixture was slowly warmed to room temperature and then stirred for 60 min. The reaction was quenched with ice-water mixture and the crude product was extracted with CH_2Cl_2 . The organic phase was separated, dried with magnesium sulfate, and volatiles were evaporated on rotavapor. The crude product was purified by column chromatography on silica (pore size 60 Å, 60–200 µm mesh particle size) using a petroleum ether/ethyl acetate (7:3) mixture as the eluent. Orange powder. Yield: 1.47 g (4.8 mmol, 44%). Mp: 113 °C. Calcd for $\text{C}_{17}\text{H}_{13}\text{FFeO}$: C, 66.27; H, 4.25. Found: C, 66.50; H, 4.39. ^1H NMR (CDCl_3 , 500 MHz, δ ppm): 7.93 (dd, $^3J(^1\text{H}, ^1\text{H}) = 8.4$ Hz, $^4J(^1\text{H}, ^{19}\text{F}) = 4.8$ Hz, 2H, C_6H_4), 7.13 (dd, $^3J(^1\text{H}, ^1\text{H}) = 8.4$ Hz, $^3J(^1\text{H}, ^{19}\text{F}) = 8.4$ Hz, 2H, C_6H_4), 4.87 (s, 2H, C_5H_4), 4.58 (s, 2H, C_5H_4), 4.19 (s, 5H, C_5H_5). $^{13}\text{C}\{^1\text{H}\}$ NMR (CDCl_3 , 125.8 MHz, δ ppm): 197.7 (s, 1C_q , CO), 165.0 (d, $^1J(^{13}\text{C}, ^{19}\text{F}) = 252.2$ Hz, 1C_q , CF), 136.1 (s, 1C_q , C_6H_4), 130.7 (d, $^3J(^{13}\text{C}, ^{19}\text{F}) = 8.6$ Hz, 2C, C_6H_4), 115.4 (d, $^2J(^{13}\text{C}, ^{19}\text{F}) = 21.6$ Hz, 2C, C_6H_4), 78.2 (s, 1C_q , C_5H_4), 72.8 (s, 2C, C_5H_4), 71.7 (s, 2C, C_5H_4), 70.4 (s, 5C, C_5H_5). IR (CH_2Cl_2): 1636 cm^{-1} ($\nu_{\text{C}=\text{O}}$). Large single crystals of **2** suitable for X-ray diffraction analysis were prepared from hexane solution by a slow evaporation of the solvent.

2.3.2. Synthesis of (4-Methoxybenzoyl)ferrocene (3)

The steps of synthesis followed the aforementioned protocol for compound **2**. Used reagents: ferrocene (2.0 g, 10.75 mmol), AlCl_3 (1.8 g, 13.5 mmol), 4-methoxybenzoyl chloride (1.9 g, 11.1 mmol). Orange powder. Yield: 1.55 g (4.8 mmol, 45%). Mp: 83 °C. Calcd for $\text{C}_{18}\text{H}_{16}\text{FeO}_2$: C, 67.53; H, 5.04. Found: C, 67.82; H, 5.34. ^1H NMR (CDCl_3 , 500 MHz, δ ppm): 7.93 (d, $^3J(^1\text{H}, ^1\text{H}) = 8.4$ Hz, 2H, C_6H_4), 6.94 (d, $^3J(^1\text{H}, ^1\text{H}) = 8.4$ Hz, 2H, C_6H_4), 4.89 (s, 2H, C_5H_4), 4.55 (s, 2H, C_5H_4), 4.19 (s, 5H, C_5H_5), 3.87 (s, 3H, OCH_3). $^{13}\text{C}\{^1\text{H}\}$ NMR (CDCl_3 , 125.8 MHz, δ ppm): 197.8 (s, 1C_q , CO), 162.6 (s, 1C_q , COCH_3), 132.8 (s, 1C_q , C_6H_4), 130.6 (s, 2C, C_6H_4), 113.6 (s, 2C, C_6H_4), 79.1 (s, 1C_q , C_5H_4), 72.5 (s, 2C, C_5H_4), 71.8 (s, 2C, C_5H_4), 70.5 (s, 5C, C_5H_5), 55.6 (s, 1C, OCH_3). IR (CHCl_3): 1630 cm^{-1} ($\nu_{\text{C}=\text{O}}$). Large single crystals of **3** suitable for X-ray diffraction analysis were prepared from hexane solution by a slow evaporation of the solvent.

2.3.3. Synthesis of (3,4,5-Trimethoxybenzoyl)ferrocene (4)

The steps of synthesis followed the aforementioned protocol for compound 2. Used reagents: ferrocene (2.0 g, 10.75 mmol), AlCl₃ (1.8 g, 13.5 mmol), 3,4,5-trimethoxybenzoyl chloride (2.6 g, 11.3 mmol). Orange powder. Yield: 1.05 g (2.8 mmol, 26%). Mp: 93 °C. Calcd for C₂₀H₂₀FeO₄: C, 63.18; H, 5.30. Found: C, 62.95; H, 5.43. ¹H NMR (CDCl₃, 500 MHz, δ ppm): 7.39 (s, 2H, C₆H₂), 4.98 (t, ³J(¹H,¹H) = 3.8 Hz, ⁴J(¹H,¹H) = 3.8 Hz, 2H, C₅H₄), 4.20 (t, ³J(¹H,¹H) = 3.8 Hz, ⁴J(¹H,¹H) = 3.8 Hz, 2H, C₅H₄), 4.01 (s, 5H, C₅H₅), 3.84 (s, 3H, OCH₃), 3.39 (s, 6H, OCH₃). ¹³C{¹H} NMR (C₆D₆, 125.8 MHz, δ ppm): 196.9 (s, 1C_q, CO), 154.1 (s, 2C_q, COCH₃), 142.9 (s, 1C_q, COCH₃), 135.7 (s, 1C_q, C₆H₄), 107.2 (s, 2C, C₆H₄), 79.9 (s, 1C_q, C₅H₄), 72.6 (s, 2C, C₅H₄), 72.2 (s, 2C, C₅H₄), 70.7 (s, 5C, C₅H₅), 60.8 (s, 1C, OCH₃), 56.2 (s, 2C, OCH₃). IR (CHCl₃): 1634 cm⁻¹ (ν_{C=O}). Large single crystals of 4 suitable for X-ray diffraction analysis were prepared from hexane solution by slow evaporation of the solvent.

2.4. Electrochemical Studies

Electrochemical study was carried out in acetonitrile (MeCN) and *N,N*-dimethylformamide (DMF), in both cases containing 0.1M Bu₄NPF₆ as a supporting electrolyte. Cyclic voltammetry (CV) and rotating disk voltammetry (RDV) were used in a three-electrode arrangement. Glassy carbon (*D* = 2 mm) was used as the working electrode for CV and RDV experiments. Saturated calomel electrode (SCE) separated by a bridge filled with supporting electrolyte and platinum sheet were used as the reference and auxiliary electrode, respectively. All potentials are given vs. SCE. Voltammetric measurements were performed using a potentiostat PGSTAT 128 N (AUTOLAB, Metrohm Autolab B.V., Utrecht, The Netherlands) operated via NOVA 1.11.2 software.

2.5. X-ray Diffraction Analysis

Crystallographic data (Table 1) were collected either on a Nonius KappaCCD diffractometer equipped with a Bruker APEX-II CCD detector by monochromatized MoKα radiation (λ = 0.71073 Å) (2 and 3) and on a Bruker D8 VENTURE Kappa Duo PHOTON100 by IμS micro-focus sealed tube MoKα radiation (λ = 0.71073 Å) (4). The structures were solved by direct methods (XP) [33] and refined by full matrix least squares based on *F*² (SHELXL2018) [34]. The hydrogen atoms on carbon were fixed into idealized positions using riding model. Temperature factors either *H*_{iso}(*H*) = 1.2 *U*_{eq}(pivot atom), or *H*_{iso}(*H*) = 1.5 *U*_{eq}(pivot atom) were assigned for the CH moiety. ORTEP drawings were made via PLATON software (University of Glasgow, Glasgow, UK).

Table 1. Summary of crystallographic data for ferrocene derivatives.

Compound	2	3	4
Formula	C ₁₇ H ₁₃ FFeO	C ₁₈ H ₁₆ FeO ₂	C ₂₀ H ₂₀ FeO ₄
<i>M_r</i>	308.12	320.16	380.21
Crystal system	Triclinic	Monoclinic	Monoclinic
Space group	<i>P</i> $\bar{1}$ (No. 2)	<i>P</i> 2 ₁ / <i>n</i> (No. 14)	<i>P</i> 2 ₁ / <i>c</i> (No. 14)
<i>a</i> (Å)	6.1079(2)	6.3152(1)	8.6322(7)
<i>b</i> (Å)	10.1461(3)	28.2133(6)	14.7211(10)
<i>c</i> (Å)	10.8772(3)	8.0592(2)	13.3636(9)
<i>α</i> (°)	81.068(1)	90	90
<i>β</i> (°)	76.508(1)	101.506(1)	101.811(2)
<i>γ</i> (°)	82.235(1)	90	90
<i>Z</i>	2	4	4
<i>V</i> (Å ³)	644.08(3)	1407.07(5)	1662.2(2)
<i>d_c</i> (g·cm ⁻³)	1.589	1.511	1.519
Crystal size	0.549 × 0.426 × 0.150	0.814 × 0.613 × 0.502	0.383 × 0.347 × 0.252
Color	Orange	Orange	Orange-red
Shape	Prism	Prism	Prism
<i>μ</i> (mm ⁻¹)	1.173	1.072	0.929

Table 1. Cont.

Compound	2	3	4
$F(000)$	316.0	664.0	792.0
h range	−7, 7	−7, 8	−11, 11
k range	−13, 9	−38, 36	−19, 19
θ range (°)	1.941, 27.498	2.678, 27.494	2.410, 27.541
Reflections measured	8228	6585	
Reflections independent (R_{int}^1)	2919 (0.0165)	3213 (0.0143)	3822 (0.0206)
Reflections observed [$I > 2\sigma(I)$]	2684	3014	3675
No. of parameters	181	191	229
GOF ²	1.044	1.119	1.075
R^3 , wR^4	0.0239, 0.0572	0.0265, 0.0621	0.0243, 0.0656
$\Delta\rho$ (e·Å ^{−3})	0.369, −0.256	0.302, −0.308	0.337, −0.465

¹ $R_{\text{int}} = \Sigma|F_o^2 - F_{o,\text{mean}}^2|/\Sigma F_o^2$; ² GOF = $[\Sigma(w(F_o^2 - F_c^2)^2)/(N_{\text{diffractions}} - N_{\text{parameters}})]^{0.5}$ for all data; ³ $R(F) = \Sigma|F_o| - |F_c|/\Sigma|F_o|$ for observed data; ⁴ $wR(F^2) = [\Sigma(w(F_o^2 - F_c^2)^2)/(\Sigma w(F_o^2)^2)]^{0.5}$ for all data.

2.6. Preparation of Test Formulations

Alkyd formulations for mechanical tests and kinetic measurements were prepared in the concentration range 0.1 to 0.03 wt.% of metal in dry matter content. The ferrocene derivatives **1**, **3** and **4** were dissolved in toluene (100 μL) and then treated with the alkyd resin (5 g). The mixtures were stirred vigorously with a spatula in glass vials and then degassed in the ultrasonic bath for 3 min. Due to very low solubility in toluene, compound **2** was pre-dissolved in CH_2Cl_2 (100 μL) instead of toluene.

2.7. Mechanical Tests

Determination of drying times and relative hardness of test coatings was performed as described previously [15]. Briefly, tack-free time (τ_1), dry-hard time (τ_2), and dry-through time (τ_3) were determined using a B. K. Drying Time Recorder (BYK, Wesel, Germany) equipped with hemispherical-ended needles ($D = 1$ mm) and 5 g weights according to ASTM D5895-03. Prepared alkyd formulations were cast on clean glass strips using a frame applicator of 76 μm gap. The measurements were done in 24-h setup under standard laboratory conditions ($T = 23$ °C, relative humidity = 50%).

Film hardness development was evaluated on coatings cast on glass plates by a frame applicator of 150 μm gap. The measurements were done on a Persoz-Pendulum Damping Tester (Elcometer, Manchester, UK) according to ISO 1522:2006 within 100 days. Relative hardness (H_{rel}) was estimated as number of swings obtained for the coated plate divided by number of swings obtained for a glass standard. The coated plates were stored under standard laboratory conditions ($T = 23$ °C, relative humidity = 50%). The measurements were done under the same conditions.

2.8. Kinetics of the Autoxidation Process

Kinetics of the chemical curing were followed by time-resolved spectroscopy in mid-infrared region. The measurements were performed on a Nicolet iS50 FTIR spectrometer (Waltham, MA, USA) using attenuated total reflection (ATR) sampling technique (64 scans per spectrum, data spacing = 0.5 cm^{-1}). The alkyd formulations were applied on a built-in diamond ATR crystal using a frame applicator of 25 μm gap. It gives coatings of 5 μm wet thickness as the crystal surface lies 20 μm above the plate, on which the frame applicator abuts. The mid-infrared spectra were recorded in the region of 4000–400 cm^{-1} every 5 min for 24 h under laboratory conditions ($T = 23$ °C; relative humidity = 50%). The data processing was done in the line with our previous studies [15]. Briefly, the intensity of $\nu_a(\text{cis-C=C-H})$ band was estimated by integration of the region 3025–2990 cm^{-1} using a fixed two-point baseline. Rate coefficients (k_{max}) at the beginning of the autoxidation process were estimated as the steepest slope of the logarithmic plots of the integrated areas vs. time. The intensity of $\omega(\text{cis-trans-C=C-H})$ band was estimated as height of the infrared band at 989 cm^{-1} using a linear baseline fixed at the region 1010–945 cm^{-1} .

3. Results and Discussion

3.1. Synthesis and Characterization of Benzoyl Substituted Ferrocenes

Ferrocenes substituted in one of the cyclopentadienyl rings by benzoyl (**1**), 4-fluorobenzoyl (**2**), 4-methoxybenzoyl (**3**) and 3,4,5-trimethoxybenzoyl group (**4**) were synthesized by a well-established protocol based on the Fiedel-Crafts acylation of ferrocene (Scheme 1) [29]. Crude products containing traces of starting ferrocene and 1,1'-disubstituted products were purified by column chromatography on silica using a petroleum ether/ethyl acetate mixture as an eluent.

Characterization of the isolated ferrocene derivatives was done by elemental analysis and spectroscopic methods. ^1H NMR spectra of the purified samples exhibit a typical pattern of monosubstituted ferrocenes (Supplementary Materials). They involve one singlet at region 4.01–4.19 ppm (5H) and two multiplets at 4.87–4.98 ppm (2H) and 4.20–4.58 ppm (2H). The species containing 1,4-disubstituted benzene rings (**2** and **3**) give two signals at 7.93 (2H) and 6.94–7.13 ppm (2H) with the interaction constant of 8.4 Hz. In the case of **2**, both NMR signals are split by a nuclear spin of ^{19}F ($I = 1/2$, 100%). The observed interaction constants (4.8 and 8.4 Hz) are consistent with monofluorinated benzenes. Singlet at 3.87 ppm, appearing in the ^1H NMR spectrum of compound **3**, has been assigned to hydrogen atoms of the methoxy group. The 3,4,5-trimethoxybenzoyl group of the compound **4**, gives three singlets at 7.39, 3.84 and 3.39 ppm. They have been assigned to hydrogen atoms of the tetrasubstituted benzene ring (2H), methoxy group in the 4-position (3H) and methoxy groups in the 3,5-positions (6H), respectively. $^{13}\text{C}\{^1\text{H}\}$ NMR spectra of the prepared compounds exhibit a pattern consistent with the proposed structures (Supplementary Materials). The signals at 70.4–70.7 ppm (5C), 71.7–72.2 ppm (2C), 72.5–72.8 ppm (2C), and 78.2–79.9 ppm (1C) have been assigned to ferrocene framework.

The presence of acyl substituents has been evidenced by infrared spectroscopy. A strong band of C=O stretching, observed in solution spectra of the compounds **1–4**, appears in a narrow range of 1630–1636 cm^{-1} . It implies only a subtle effect of given substitution pattern on electronic properties of the central metal. Such observation is in line with results of electrochemical study focused on structure/redox properties relationship, revealing only subtle differences in ferrocene oxidation among the compounds **1–4**; see Figure 1 and data in Table 2. For comparison, the cyclic voltammetry was measured in two solvents; acetonitrile and dimethyl formamide. The first oxidation of the studied compounds proceeds as one-electron reversible process ascribed to ferrocene/ferrocenium redox couple. Its potential is shifted anodically of ca. 270 mV in comparison to oxidation of unsubstituted ferrocene due to the presence of the electron-withdrawing benzoyl group. The electrochemical data of the compound **1** are consistent with those published previously [35]. The observed subtle differences in ferrocene oxidation within species **1–4** can be attributed to changes in geometry discussed below. In the case of compound **4**, another irreversible oxidation process is registered at potential +1.67 V, probably corresponding to oxidation of methoxy substituents.

Table 2. Electrochemical data of studied ferrocene derivatives.

Compound	E^{of} (ox1) [V] ¹	E^{of} (red1) [V] ¹	ΔE [V] ²
	MeCN/DMF	MeCN/DMF	MeCN/DMF
1	0.67/0.70	−1.93/−1.91	2.61/2.61
2	0.65/0.70	−1.95/−1.90	2.61/2.61
3	0.63/0.68	−2.04/−2.02	2.67/2.69
4	0.65/0.69	−1.95/−1.92	2.60/2.61

¹ $E^{\text{of}} = (E_{\text{p,c}} + E_{\text{p,a}})/2$, for which $E_{\text{p,c}}$ and $E_{\text{p,a}}$ correspond to the cathodic and anodic peak potentials, respectively. All potentials vs. SCE were obtained by CV; ² $\Delta E = E^{\text{of}}(\text{ox1}) - E^{\text{of}}(\text{red1})$.

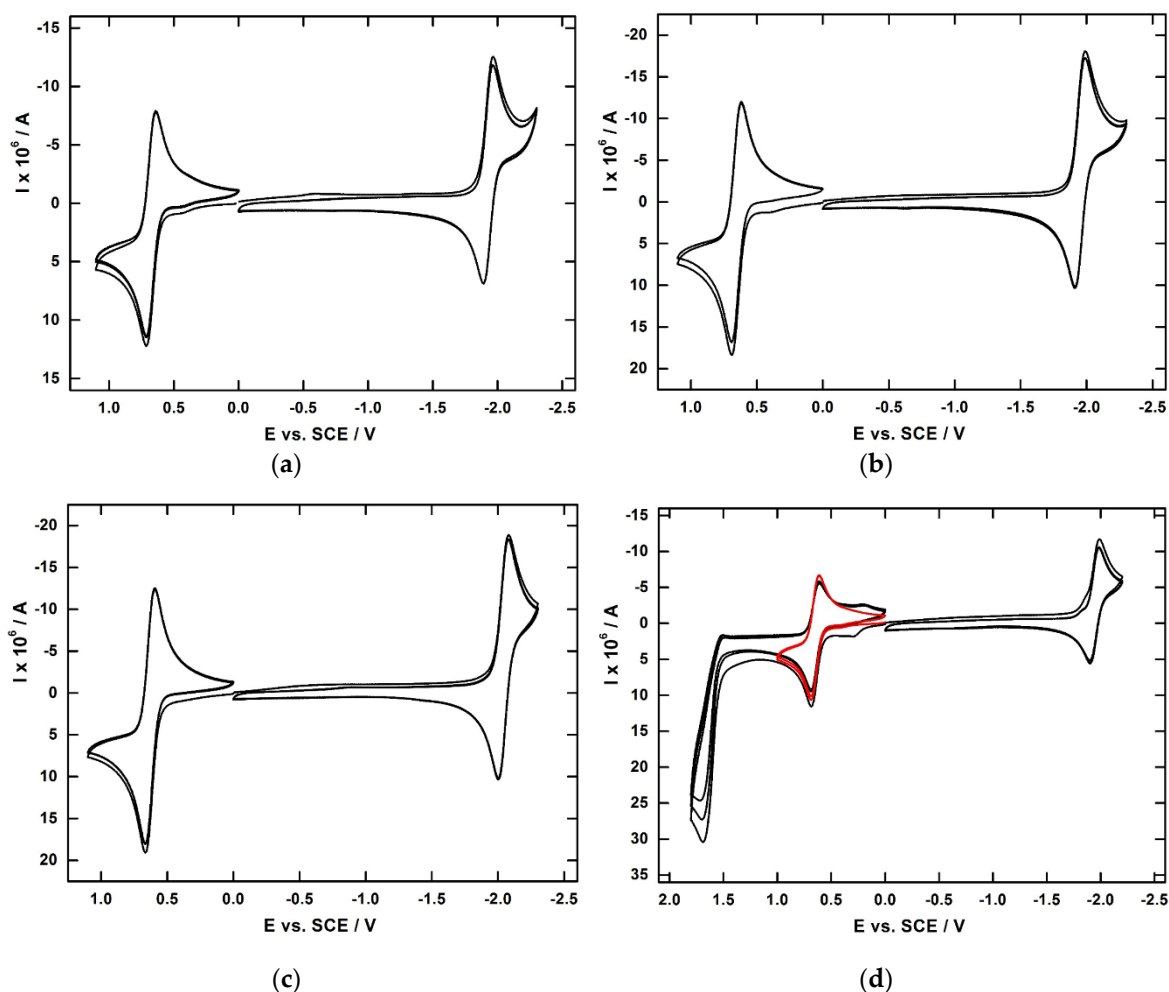


Figure 1. Cyclic voltammetry acetonitrile of compounds **1** (a), **2** (b), **3** (c) and **4** (d) containing 0.1 M Bu_4NPF_6 at glassy carbon electrode. $\nu = 100 \text{ mV}\cdot\text{s}^{-1}$.

The first reduction of compounds **1–4** proceeds also as one-electron reversible process, which can be explained as the formation of stable radical anion localized at carbonyl group. It is noteworthy that the presence of fluoro (**2**) or methoxy substituents (**3**, **4**) does not play a significant role in the reduction. The difference between first oxidation and first reduction potential ΔE , correlating with HOMO/LUMO gap, shows similar values within the series. The only exception is compound **3** where the highest value of ΔE points to lower delocalization of electron density.

In comparison of compounds studied herein with previously published data for vanadium based driers [19], it can be stated that compounds **1–4** are more easily oxidized than $[\text{VO}(\text{acac})_3]$ and its congeners, while oxidized forms of the vanadium compounds are stronger oxidants.

Structures of the compounds **2–4** have been determined by X-ray diffraction analysis on single crystals prepared by solvent evaporation technique (Figure 2). The molecules have a typical sandwich structure with two parallel cyclopentadienyl rings η^5 -bonded to iron atom in a formal oxidation state II. Distance between the iron atom and a centroid of the substituted cyclopentadienyl ring is considerably shorter [Fe–Cg1: 1.6426(8)–1.6489(7) Å] than in the case of the unsubstituted ring [Fe–Cg2: 1.6508(8)–1.6563(6) Å], see Table 3. It is attributed to strong electron-withdrawing properties of the acyl substituents that strengthen a back-donation of iron *d*-electrons to antibonding π -orbitals of the cyclopentadienyl ligand. In all compounds under the study, cyclopentadienyl ring is not fully conjugated with C=O group. It is evidenced from the dihedral angle between a plane of the cyclopentadienyl ring and a plane of the acyl function (defined by C11, C12, C13 and O1), see parameter

α in Table 3. A degree of conjugation between the C=O group and benzene ring was found to be even lower as revealed from higher values of the parameter β given in Table 3.

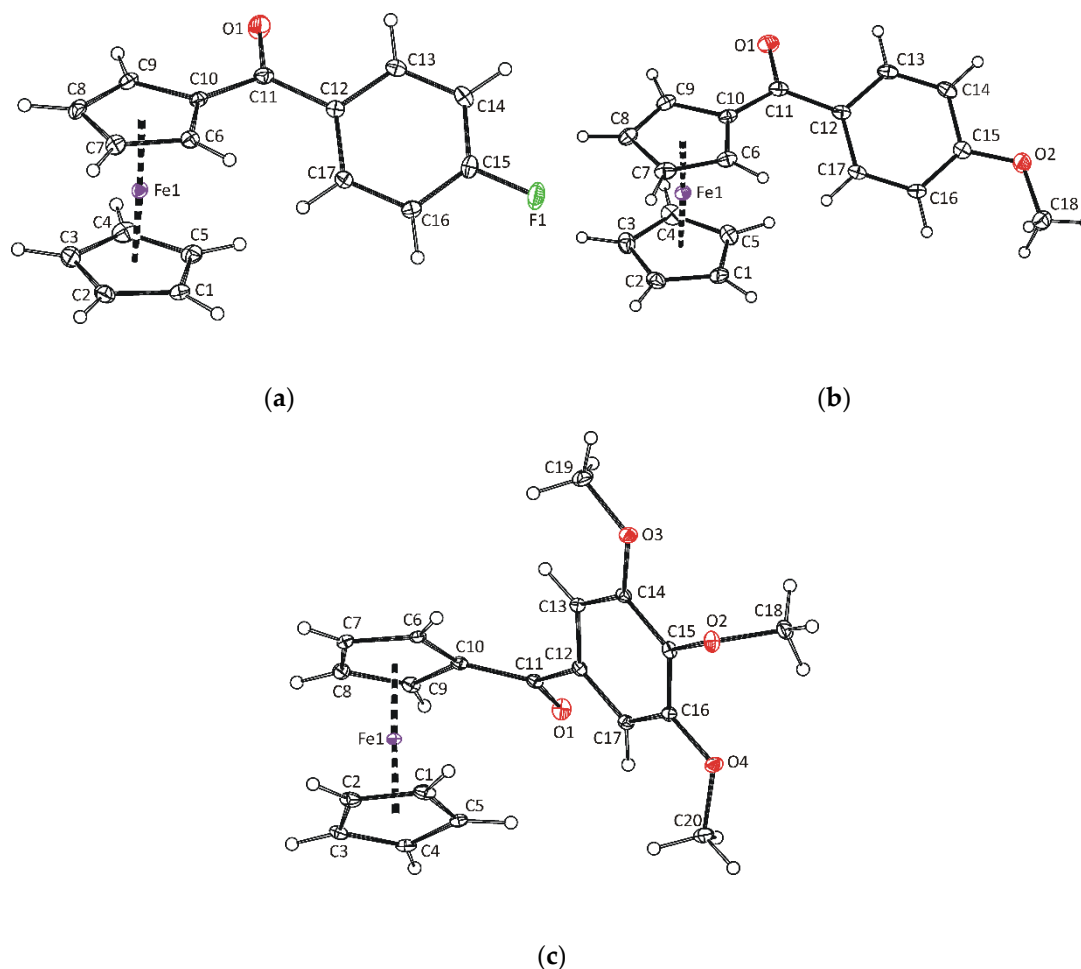


Figure 2. ORTEP drawings of: (a) $[(\eta^5\text{-C}_5\text{H}_4\text{COC}_6\text{H}_4\text{F-4})(\eta^5\text{-C}_5\text{H}_5)\text{Fe}]$ present in crystal structure of **2**; (b) Molecules of $[(\eta^5\text{-C}_5\text{H}_4\text{COC}_6\text{H}_4\text{OMe-4})(\eta^5\text{-C}_5\text{H}_5)\text{Fe}]$ present in the crystal structure of **3**; (c) Molecules of $[(\eta^5\text{-C}_5\text{H}_4\text{COC}_6\text{H}_2(\text{OMe})_{3-3,4,5})(\eta^5\text{-C}_5\text{H}_5)\text{Fe}]$ present in crystal structure of **4**. Thermal ellipsoids are drawn at the 30% probability level.

Table 3. Selected geometric parameters for ferrocene derivatives **1–4**¹.

Parameter	1 ²	2	3	4
Fe–Cg1 ³	1.6464(10)	1.6489(7)	1.6426(8)	1.6454(6)
Fe–Cg2 ⁴	1.6549(12)	1.6517(7)	1.6508(8)	1.6563(6)
Cg1–Fe–Cg2 ^{3,4}	177.57(6)	177.86(4)	177.68(5)	177.46(3)
α ⁵	14.26(13)	17.60(9)	15.18(9)	10.84(8)
β ⁶	26.20(13)	25.29(8)	23.60(8)	44.75(7)

¹ Bond lengths and bond angles are given in Å and °, respectively; ² Data reported elsewhere [36]; ³ Cg1 is center of gravity of C6–C10; ⁴ Cg2 is center of gravity of C1–C5; ⁵ Dihedral angle between planes defined by ring C6–C10 and atoms C10, C11, C12, O1; ⁶ Dihedral angle between planes defined by ring C12–C17 and atoms C10, C11, C12, O1.

3.2. Room Temperature Curing of Alkyd Resin

The catalytic activity toward room temperature curing of alkyd resins was evaluated on solvent-borne binder modified with soybean oil. Tack-free time (τ_1), dry-hard time (τ_2) and dry-through time (τ_3) of test coatings were estimated by Beck–Koller methods according to ASTM D5895-03.

Their relative hardness was measured by dumping test using Persoz-type pendulum in line with ISO 1522:2006. Samples **1**, **3** and **4** were pre-dissolved in toluene immediately before formulation while **2** was pre-dissolved in dichloromethane, owing to its much lower solubility in nonpolar solvents. The results of the mechanical tests for ferrocenes **1–4** are summarized in Table 4 together with data for commercial cobalt-based drier (**Co-2EH**).

Table 4. Drying times of test coatings and development of their hardness.

Drier	Metal Content (wt.%)	τ_1 ¹ (h)	τ_2 ² (h)	τ_3 ³ (h)	$H_{rel,10d}$ ⁴ (%)	$H_{rel,100d}$ ⁵ (%)
1	0.1	10.1	12.1	12.1	24.9	41.9
	0.06	19.7	21.6	21.6	24.7	41.6
	0.03	>24	>24	>24	– ⁶	– ⁶
2	0.1	5.8	7.7	9.2	25.6	40.5
	0.06	14.1	17.2	>24	25.4	39.7
	0.03	>24	>24	>24	– ⁶	– ⁶
3	0.1	0.9	4.5	5.1	27.0	39.7
	0.06	4.0	5.5	7.2	26.6	39.1
	0.03	9.7	14.5	16.9	– ⁶	– ⁶
4	0.1	16.4	18.8	18.8	28.6	42.0
	0.06	22.5	>24	>24	26.0	40.8
	0.03	>24	>24	>24	– ⁶	– ⁶
Co-2EH	0.1	0.9	5.5	5.5	25.9	61.2
	0.06	2.7	8.1	8.1	35.3	53.5
	0.03	7.9	11.3	>24	– ⁶	– ⁶

¹ Tack-free time; ² Dry-hard time; ³ Dry-through (total-dry) time; ⁴ Relative hardness measured after 10 days of curing; ⁵ Final relative hardness; ⁶ Not measured.

Interestingly, activity of modified benzoylferrocenes strongly depends on substitution in benzene ring even through differences in redox potential of the system Fe^{II}/Fe^{III} are negligible. At 0.1 wt.%, the catalytic activity of the ferrocenes increases in line **4** < **1** < **2** < **3**, as revealed from comparison of drying times τ_1 – τ_3 listed in Table 4. At this concentration, parent benzoylferrocene (**1**) exhibits a longer dry-hard time (τ_3) than **Co-2EH** and its activity further decreases with decreasing concentration. We note that here reported drying times of **1** are considerably longer than those estimated previously [27], which is probably due to different alkyd baths and modified process of sample preparation. In the current study, we tried to exclude the effect of dimethyl sulfoxide that was used in the previous study for pre-dissolution of **1**, since such coordinating solvent could promote decomposition of ferrocene framework upon long-term storage.

Fast curing of the alkyd coatings was observed for the formulations containing derivative **3**. At concentration 0.1 wt.%, this drier seems to be very powerful as the drying times near the values obtained for commercial **Co-2EH** (Table 4). Similarly as in case of the cobalt-based drier, derivative **3** exhibits a high catalytic activity even at concentration 0.06 wt.% and considerable prolongation of the drying times is not evidenced before metal concentration 0.03 wt.%.

Long term curing of the test coatings was followed by development of relative hardness that was estimated by dumping test using Persoz-type pendulum [37]. The coatings treated with the ferrocenes **1–4** reach 24.7–27.0% hardness of the glass standard within 10 days. The hardening process continues up to final values of 39.7–42.0%. The substitution in the benzene ring of the benzoylferrocene has only a subtle effect on the relative hardness development as evident from values of $H_{rel,10d}$ and $H_{rel,100d}$ listed in Table 4. The effect of metal concentration seem to be also negligible; at least in the range 0.06–0.1 wt.% as shown in Figure 3. It is noteworthy that final hardness ($H_{rel,100d}$) is lower than in the case of coatings cured with **Co-2EH**, which is a common feature of the driers used as cobalt replacement [38].

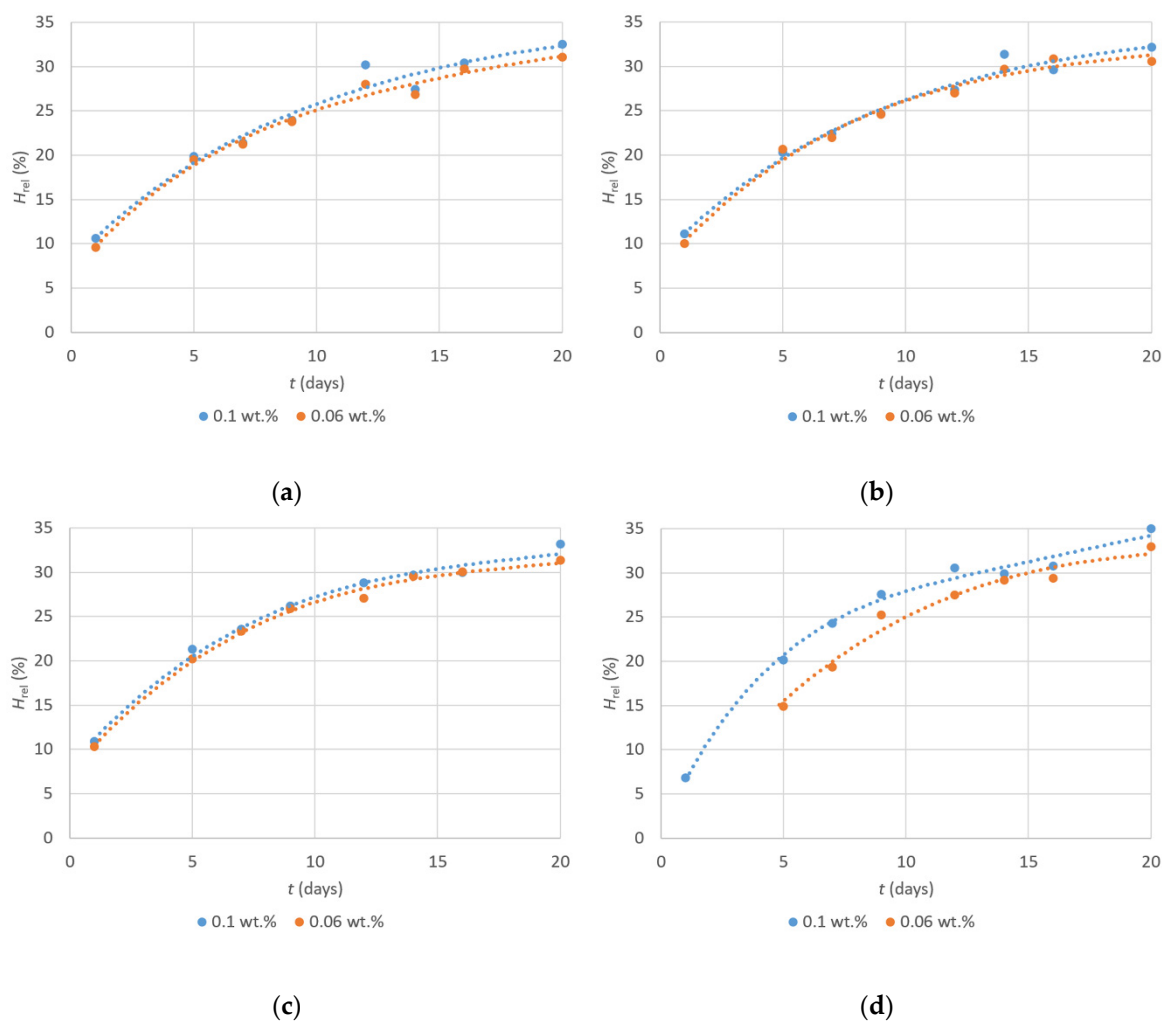


Figure 3. Effect of concentration on development of the relative hardness of test coatings cured by compounds **1** (a), **2** (b), **3** (c) and **4** (d).

3.3. Kinetic Studies on the Substituted Ferrocenes

The effect of substitution on the catalytic activity of benzoylferrocene was further investigated by infrared spectroscopy. The time-resolved arrangement is capable to follow peroxidation of unsaturated fatty acids, which is the first step of chemical curing of alkyd-based paints [12]. Time development of the allylic C–H stretching band $\nu_a(\text{cis-C}=\text{C-H})$, observed at 3008 cm^{-1} , follows consumption of the reactive unsaturated substrate ($\alpha = 1 - A_t/A_0$) as established in previous studies on model systems for air-drying paints [39]. Conjugated system of double bonds generates vibration mode $\omega(\text{cis-trans-C}=\text{C-H})$, appearing as a characteristic band at 989 cm^{-1} [18]. This absorption band rises in time as peroxidation step of the autoxidation proceeds. It reaches a maximum at t_{conj} and then intensity of the band decreases owing to proceeding radical additions, which is the main process responsible for alkyd crosslinking [12].

In the current study, we decided to investigate the peroxidation process directly on a thin layer of alkyd resin using ATR sampling technique. It enables to exclude the effect of oxygen diffusion into the coatings and follow the catalytic power of the drier in a sample saturated with air-oxygen [40]. The kinetic study was performed with samples of ferrocenes **1**, **3** and **4** pre-dissolved in toluene. We note that derivative **2** was excluded from the study owing its very low solubility.

Figure 4a shows an intensity decrease of the stretching band $\nu_a(\text{cis-C}=\text{C-H})$. The plot in the linear scale reflects a conversion of the substrate to hydroperoxides. The time, when the absorbance drops to

50% of its initial value, is taken as a half-life of the peroxidation process ($t_{1/2}$, Table 5). The peroxidation of fatty acids can be taken as a reaction of pseudo-first order as evidenced previously on ethyl linoleate saturated with air-oxygen taken as a simplified model for the air-drying paints [39]. A very similar behavior has been documented on a thin layer of air-drying binders [40]. In the case of formulations treated with ferrocene derivatives, described here, the peroxidation step proceeds as a typical reaction of the pseudo-first order as documented by the logarithmic plots given in Figure 4b. Linear region is observed up to $A_t/A_0 \approx 0.35$ ($\alpha \approx 65\%$). At higher conversions, the process slows down considerably as the sol-gel transition proceeds. Estimated reaction rates (k_{\max}) and induction times (IT) for systems under the study are summarized in Table 5.

At concentration 0.1 wt.%, ferrocene derivatives **1**, **3** and **4** show rate constant of the peroxidation reaction 0.30, 0.25 and 0.23 h^{-1} , respectively. Although the values are much lower than in the case of the drier **Co-2EH** (2.18 h^{-1}) [15], they seem to be high enough for paint applications. Hence, differences in the rates of drying, documented by the mechanical tests, are apparently caused by variation of the induction period. At given concentration, IT increases in the line $3 < 1 < 4$, which well correlates with prolongation of the drying time revealed by mechanical tests. Lowering of metal concentration leads to a decrease of the rate constant and a prolongation of the induction period. Nevertheless, the derivative **3** at concentration 0.03 wt.% exhibits still acceptable value of IT (3.0 h), which clarifies considerably better performance in mechanical tests than observed for the compounds **1** and **4**.

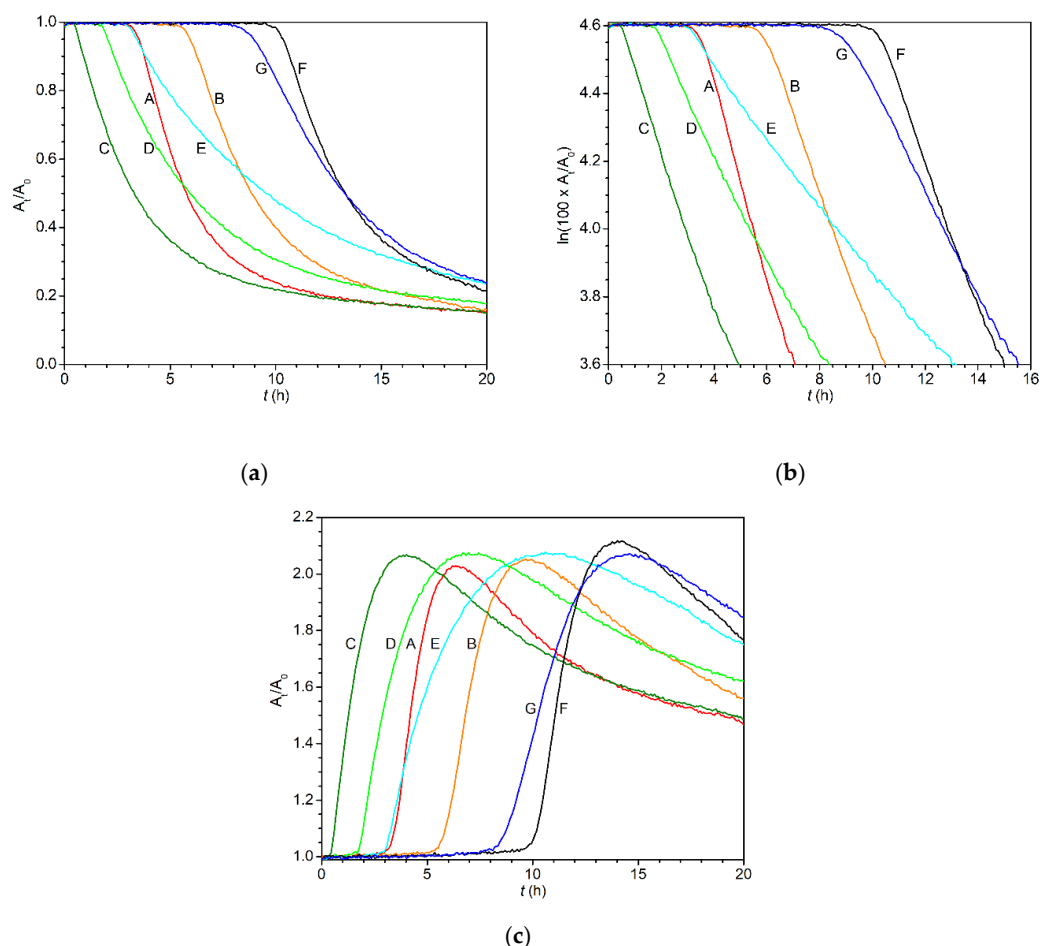


Figure 4. Time development of the infrared band: (a) at 3008 cm^{-1} in linear scale; (b) at 3008 cm^{-1} in logarithmic scale; (c) at 989 cm^{-1} in linear scale. A: 1/0.1 wt.%, B: 1/0.06 wt.%; C: 3/0.1 wt.%, D: 3/0.06 wt.%, E: 3/0.03 wt.%, F: 4/0.1 wt.%, G: 4/0.06 wt.%.

Table 5. Kinetic parameters for ferrocene derivatives.

Drier	Metal Content (wt.%)	k_{\max}^1 (h ⁻¹)	IT ¹ (h)	$t_{1/2}^1$ (h)	t_{conj}^2 (h)
1	0.1	0.30	3.4	5.8	6.5
	0.06	0.24	5.7	8.9	9.8
3	0.1	0.25	0.5	3.3	4.0
	0.06	0.18	1.8	5.9	7.4
	0.03	0.12	3.0	9.5	11.0
4	0.1	0.23	10.3	13.3	14.1
	0.06	0.16	8.9	13.2	14.7
Co-2EH³	0.1	2.18	0.2	0.5	0.6
	0.06	1.55	0.5	0.9	1.0

¹ Maximum rate constant (k_{\max}), induction time (IT) and half-life ($t_{1/2}$) of autoxidation process; ² Time, in which content of *cis-trans* conjugated double bonds reached maximum; ³ Data reported elsewhere [15].

Development of intensity of the vibration mode $\omega(\text{cis-trans-C=C-H})$ is given in Figure 4c. It documents a fast rise of the conjugated double bonds concentration upon the peroxidation step, which is followed by a slow decrease due to crosslinking reaction. The time, when crosslinking prevails over the peroxidation process, is denoted as t_{conj} . The values t_{conj} , listed in Table 5, show a similar trend as observed for $t_{1/2}$. At a given concentration, they increase in the line: **Co-2EH** < **3** < **1** < **4**.

4. Conclusions

This study has described changes in catalytic power of alkyd driers induced by subtle modification. The substitution effect has been demonstrated on derivatives of ferrocene, which was chosen due to its unique structure, chemical inertness and a pronounced Fe^{II}/Fe^{III} redox couple. Purity of synthesized ferrocene compounds 1–4 has been checked by standard analytical tools. Identity of derivatives 2–4, not available in literature sources, has been elucidated from ¹H and ¹³C{¹H}NMR spectra and unambiguously confirmed by X-ray diffraction analysis on single crystals.

Mechanical tests on alkyd coatings have revealed unusually large differences in drying times related with subtle modification of the ferrocene periphery. The observed variation of the catalytic activity is not related with redox power of the driers since substitution of the benzene ring in benzoylferrocene has a negligible effect on the Fe^{II}/Fe^{III} redox couple as evidenced by cyclic voltammetry. The effect of hydroperoxide coordination has also been excluded as ferrocene derivatives were pronounced as coordinatively and electronically saturated molecules not undergoing ligand-exchange reactions under mild conditions. Kinetic studies, focused on the alkyd peroxidation step, have pointed to the fact that improved activity of the derivative 3 is not a result of higher rate constants, as one should suggest, but is related with faster initiation of the process as documented by observed induction times.

In summary, this work has shown that modification of currently known ferrocene-based driers can lead to species with properties comparable or even superior to currently used cobalt carboxylates.

Supplementary Materials: The following are available online at <http://www.mdpi.com/2079-6412/10/9/873/s1>. Figure S1: ¹H and ¹³C{¹H} NMR spectra of the compound 2, Figure S2: ¹H and ¹³C{¹H} NMR spectra of the compound 3, Figure S3: ¹H and ¹³C{¹H} NMR spectra of the compound 4, CCDC 1993692–1993694 contain crystallographic data for this contribution. These data can be obtained free of charge from Cambridge Crystallographic Data Centre via www.ccdc.cam.ac.uk/data_request/cif.

Author Contributions: Conceptualization, J.H.; synthesis of the compounds, J.H.; testing of the compounds, T.F.; electrochemistry—data collection and analysis, T.M.; X-ray diffraction—data collection and analysis, I.C.; writing—original draft preparation, J.H.; writing—review and editing, J.H.; supervision, J.V.; project administration, J.V. All authors have read and agreed to the published version of the manuscript.

Funding: This research received no external funding.

Conflicts of Interest: The authors declare no conflict of interest.

References

1. Astruc, D. Why is Ferrocene so Exceptional? *Eur. J. Inorg. Chem.* **2017**, *2017*, 6–29. [[CrossRef](#)]
2. Dai, L.X.; Tu, T.; You, S.L.; Deng, W.P.; Hou, X.L. Asymmetric Catalysis with Chiral Ferrocene Ligands. *Acc. Chem. Res.* **2003**, *36*, 659–667. [[CrossRef](#)] [[PubMed](#)]
3. Arrayás, R.G.; Adrio, J.; Carretero, J.C. Recent Applications of Chiral Ferrocene Ligands in Asymmetric Catalysis. *Angew. Chem. Int. Ed.* **2006**, *45*, 7674–7715. [[CrossRef](#)] [[PubMed](#)]
4. Tong, R.; Zhao, Y.; Wang, L.; Yu, H.; Ren, F.; Saleem, M.; Amer, W.A. Recent research progress in the synthesis and properties of burning rate catalysts based on ferrocene-containing polymers and derivatives. *J. Organomet. Chem.* **2014**, *755*, 16–32. [[CrossRef](#)]
5. Li, L.; Shi, J.L.; Yan, J.N.; Zhao, X.G.; Chen, H.G. Mesoporous SBA-15 material functionalized with ferrocene group and its use as heterogeneous catalyst for benzene hydroxylation. *Appl. Catal. A Gen.* **2004**, *263*, 213–217. [[CrossRef](#)]
6. Wang, Q.; Tian, S.; Ning, P. Ferrocene-Catalyzed Heterogeneous Fenton-like Degradation of Methylene Blue: Influence of Initial Solution pH. *Ind. Eng. Chem. Res.* **2014**, *53*, 6334–6340. [[CrossRef](#)]
7. Li, Y.; Zhang, B.; Liu, X.; Zhao, Q.; Zhang, H.; Zhang, Y.; Ning, P.; Tian, S. Ferrocene-catalyzed heterogeneous Fenton-like degradation mechanisms and pathways of antibiotics under simulated sunlight: A case study of sulfamethoxazole. *J. Hazard. Mater.* **2018**, *353*, 26–34. [[CrossRef](#)]
8. Andrew Lin, K.Y.; Lin, T.Y.; Chena, Y.C.; Lin, Y.F. Ferrocene as an efficient and recyclable heterogeneous catalyst for catalytic ozonation in water. *Catal. Commun.* **2017**, *95*, 40–45. [[CrossRef](#)]
9. Yamaguchi, Y.; Kotal, C. Benzoyl-Substituted Ferrocenes: An Attractive New Class of Anionic Photoinitiators. *Macromolecules* **2000**, *33*, 1152–1156. [[CrossRef](#)]
10. Sanderson, C.T.; Palmer, B.J.; Morgan, A.; Murphy, M.; Dluhy, R.A.; Mize, T.; Amster, I.J.; Kotal, C. Classical Metallocenes as Photoinitiators for the Anionic Polymerization of an Alkyl 2-Cyanoacrylate. *Macromolecules* **2002**, *35*, 9648–9652. [[CrossRef](#)]
11. Jones, F.N. Alkyd Resins. In *Ullmann's Encyclopedia of Industrial Chemistry*; Wiley-VCH Verlag: Weinheim, Germany, 2003. [[CrossRef](#)]
12. Honzík, J. Curing of Air-Drying Paints: A Critical Review. *Ind. Eng. Chem. Res.* **2019**, *58*, 12485–12505. [[CrossRef](#)]
13. Leyssens, L.; Vinck, B.; Van Der Straeten, C.; Wuyts, F.; Maes, L. Cobalt toxicity in humans—A review of the potential sources and systemic health effects. *Toxicology* **2017**, *387*, 43–56. [[CrossRef](#)]
14. Simpson, N.; Maaijen, K.; Roelofsen, Y.; Hage, R. The Evolution of Catalysis for Alkyd Coatings: Responding to Impending Cobalt Reclassification with Very Active Iron and Manganese Catalysts, Using Polydentate Nitrogen Donor Ligands. *Catalysts* **2019**, *9*, 825. [[CrossRef](#)]
15. Matušková, E.; Honzík, J. Performance of Manganese(III) Acetylacetonate in Solvent-Borne and High-Solid Alkyd Formulations. *Materials* **2020**, *13*, 642. [[CrossRef](#)] [[PubMed](#)]
16. Bouwman, E.; van Gorkum, R. A study of new manganese complexes as potential driers for alkyd paints. *J. Coat. Technol. Res.* **2007**, *4*, 491–503. [[CrossRef](#)]
17. de Boer, J.W.; Wesenhagen, P.V.; Wenker, E.C.M.; Maaijen, K.; Gol, F.; Gibbs, H.; Hage, R. The Quest for Cobalt-Free Alkyd Paint Driers. *Eur. J. Inorg. Chem.* **2013**, 3581–3591. [[CrossRef](#)]
18. Křížan, M.; Vinklár, J.; Erben, M.; Čisářová, I.; Honzík, J. Autoxidation of alkyd resins catalyzed by iron(II) bispidine complex: Drying performance and in-depth infrared study. *Prog. Org. Coat.* **2017**, *111*, 361–370. [[CrossRef](#)]
19. Preininger, O.; Vinklár, J.; Honzík, J.; Mikysek, T.; Erben, M. A promising drying activity of environmentally friendly oxovanadium(IV) complexes in air-drying paints. *Prog. Org. Coat.* **2015**, *88*, 191–198. [[CrossRef](#)]
20. Preininger, O.; Honzík, J.; Kalenda, P.; Vinklár, J. Drying activity of oxovanadium(IV) 2-ethylhexanoate in solvent-borne alkyd paints. *J. Coat. Technol. Res.* **2016**, *13*, 479–487. [[CrossRef](#)]
21. Preininger, O.; Charamzová, I.; Vinklár, J.; Čisářová, I.; Honzík, J. Oxovanadium(IV) complexes bearing substituted pentane-2,4-dionate ligands: Synthesis, structure and drying activity in solvent-borne alkyd paints. *Inorg. Chim. Acta* **2017**, *462*, 16–22. [[CrossRef](#)]
22. Charamzová, I.; Machálková, A.; Vinklár, J.; Čisářová, I.; Honzík, J. Benzyl substituted oxovanadium(IV) pentane-2,4-dionates: Synthesis, structure and drying properties. *Inorg. Chim. Acta* **2019**, *492*, 243–248. [[CrossRef](#)]

23. Charamzová, I.; Vinklárek, J.; Kalenda, P.; Honzíček, J. Application of Oxovanadium Complex Stabilized by *N,N,N,N*-Chelating Ligand in Air-Drying Paints. *Coatings* **2018**, *8*, 204. [CrossRef]
24. Charamzová, I.; Vinklárek, J.; Kalenda, P.; Císařová, I.; Honzíček, J. Oxidovanadium(V) dithiocarbamates as driers for alkyd binders. *J. Coat. Technol. Res.* **2020**. [CrossRef]
25. Stava, V.; Erben, M.; Vesely, D.; Kalenda, P. Properties of metallocene complexes during the oxidative crosslinking of air drying coatings. *J. Phys. Chem. Solids* **2007**, *68*, 799–802. [CrossRef]
26. Erben, M.; Veselý, D.; Vinklárek, J.; Honzíček, J. Acyl-substituted ferrocenes as driers for solvent-borne alkyd paints. *J. Mol. Catal. A Chem.* **2012**, *353–354*, 13–21. [CrossRef]
27. Honzíček, J.; Vinklárek, J. Chemical curing of alkyd resin catalyzed by benzoylferrocene: Performance, kinetics, and thickness effects. *J. Appl. Polym. Sci.* **2018**, *135*, 46184. [CrossRef]
28. Armarego, W.L.F.; Perrin, D.D. *Purification of Laboratory Chemicals*; Butterworth-Heinemann: Oxford, UK, 1996.
29. Lu, B.; Wang, Q.; Zhao, M.; Xie, X.; Zhang, Z. Ruthenium-Catalyzed Enantioselective Hydrogenation of Ferrocenyl Ketones: A Synthetic Method for Chiral Ferrocenyl Alcohols. *J. Org. Chem.* **2015**, *80*, 9563–9569. [CrossRef]
30. Greenberg, J.A.; Sammakia, T. The Conversion of *tert*-Butyl Esters to Acid Chlorides Using Thionyl Chloride. *J. Org. Chem.* **2017**, *82*, 3245–3251. [CrossRef]
31. Zaragoza, F. One-Step Conversion of Methyl Ketones to Acyl Chlorides. *J. Org. Chem.* **2015**, *80*, 10370–10374. [CrossRef]
32. Ghinet, A.; Rigo, B.; Hénichart, J.P.; Le Broc-Ryckewaert, D.; Pommery, J.; Pommery, N.; Thuru, X.; Quesnel, B.; Gautret, P. Synthesis and biological evaluation of phenstatin metabolites. *Bioorg. Med. Chem.* **2011**, *19*, 6042–6054. [CrossRef]
33. Sheldrick, G.M. SHELXT—Integrated space-group and crystal-structure determination. *Acta Crystallogr. Sect. A Found. Adv.* **2015**, *71*, 3–8. [CrossRef] [PubMed]
34. Sheldrick, G.M. Crystal structure refinement with SHELXL. *Acta Crystallogr. Sect. C Struct. Chem.* **2015**, *71*, 3–8. [CrossRef] [PubMed]
35. Khobragade, D.A.; Mahamulkar, S.G.; Pospíšil, L.; Císařová, I.; Rulišek, L.; Jahn, U. Acceptor-Substituted Ferrocenium Salts as Strong, Single-Electron Oxidants: Synthesis, Electrochemistry, Theoretical Investigations, and Initial Synthetic Application. *Chem. Eur. J.* **2012**, *18*, 12267–12277. [CrossRef] [PubMed]
36. Butler, I.R.; Cullen, W.R.; Rettig, S.J.; Trotter, J. Structure of Benzoylferrocene. *Acta Crystallogr. Sect. C Struct. Chem.* **1988**, *44*, 1666–1667. [CrossRef]
37. Persoz, B. The hardness pendulum. *Peint. Pigment. Vernis* **1945**, *21*, 194–201.
38. Gezici-Koç, Ö.; Thomas, C.A.A.M.; Michel, M.E.B.; Erich, S.J.F.; Huinink, H.P.; Flapper, J.; Duivenvoorde, F.L.; van der Ven, L.G.J.; Adan, O.C.G. In-depth study of drying solvent-borne alkyd coatings in presence of Mn and Fe-based catalysts as cobalt alternatives. *Mater. Today Commun.* **2016**, *7*, 22–31. [CrossRef]
39. van Gorkum, R.; Bouwman, E.; Reedijk, J. Fast Autoxidation of Ethyl Linoleate Catalyzed by [Mn(acac)₃] and Bipyridine: A Possible Drying Catalyst for Alkyd Paints. *Inorg. Chem.* **2004**, *43*, 2456–2458. [CrossRef]
40. Charamzová, I.; Vinklárek, J.; Honzíček, J. Effect of primary driers on oxidative drying of high-solid alkyd binder: Investigation of thickness effects by mechanical tests and infrared spectroscopy. *Prog. Org. Coat.* **2018**, *125*, 177–185. [CrossRef]



© 2020 by the authors. Licensee MDPI, Basel, Switzerland. This article is an open access article distributed under the terms and conditions of the Creative Commons Attribution (CC BY) license (<http://creativecommons.org/licenses/by/4.0/>).